THE GERONTOLOGICAL SOCIETY OF AMERICA®

Journals of Gerontology: Biological Sciences
cite as: *J Gerontol A Biol Sci Med Sci*, 2018, Vol. 73, No. 1, 29–38
doi:10.1093/gerona/glx024
Advance Access publication March 8, 2017

OXFORD

Original Article

Caloric Restriction and Rapamycin Differentially Alter Energy Metabolism in Yeast

Kyung-Mi Choi,[1] Seok-Jin Hong,[2] Jan M. van Deursen,[3] Sooah Kim,[4] Kyoung Heon Kim,[4] and Cheol-Koo Lee[1,2]

[1]Institute of Animal Molecular Biotechnology, Korea University and [2]Division of Biotechnology, College of Life Sciences & Biotechnology, Korea University, Seoul, Republic of Korea. [3]Departments of Biochemistry and Molecular Biology and Pediatric and Adolescent Medicine, Mayo Clinic, Rochester, Minnesota. [4]Department of Biotechnology, Graduate School, Korea University, Seoul, Republic of Korea.

Address correspondence to Cheol-Koo Lee, PhD, Division of Biotechnology, College of Life Sciences & Biotechnology, Korea University, Seoul 02841, Republic of Korea. E-mail: cklee2005@korea.ac.kr

Received July 26, 2016; Editorial Decision Date January 27, 2017

Decision Editor: Rafael de Cabo, PhD

Abstract

Rapamycin (RM), a drug that inhibits the mechanistic target of rapamycin (mTOR) pathway and responds to nutrient availability, seemingly mimics the effects of caloric restriction (CR) on healthy life span. However, the extent of the mechanistic overlap between RM and CR remains incompletely understood. Here, we compared the impact of CR and RM on cellular metabolic status. Both regimens maintained intracellular ATP through the chronological aging process and showed enhanced mitochondrial capacity. Comparative transcriptome analysis showed that CR had a stronger impact on global gene expression than RM. We observed a like impact on the metabolome and identified distinct metabolites affected by CR and RM. CR severely reduced the level of energy storage molecules including glycogen and lipid droplets, whereas RM did not. RM boosted the production of enzymes responsible for the breakdown of glycogen and lipid droplets. Collectively, these results provide insights into the distinct energy metabolism mechanisms induced by CR and RM, suggesting that these two anti-aging regimens might extend life span through distinctive pathways.

Keywords: Transcriptomics—Metabolomics

Caloric restriction (CR) has been demonstrated as a robust and reproducible method for extending life span in various organisms (1). The scientific community has actively searched for simpler methods for extending life span; rapamycin (RM) has been shown to successfully extend life span in various models, including yeast, worm, fly, and mouse models (2,3), suggesting that RM is a promising candidate for human life-span extension. Our recent study showed that RM maximally extended chronological life span (CLS) at a nanomolar concentration in budding yeast (2).

Previous studies have identified target of rapamycin (TOR) as the target protein of RM. In budding yeast, two different TOR proteins are encoded by the *TOR1* and *TOR2* genes. These two proteins contribute to the formation of functionally distinct complexes known as TOR complex 1 (TORC1) and TOR complex 2 (TORC2) (4). Either TOR protein can act as the main component of TORC1, whereas only TOR2 protein can function as the main component of TORC2. TORC1 is RM-sensitive and regulates various cellular processes including translation, ribosomal biogenesis, and autophagy (5). TORC2 is involved in actin organization and is thought to be RM-insensitive; however, recent work has shown that long-term RM treatment can also inhibit TORC2 (6).

A CR-mediated life-span extension mechanism has been shown to be associated with the TOR pathway; thus, it has been hypothesized that RM and CR increase life span through similar mechanisms. For example, a TOR1 mutation in *Saccharomyces cerevisiae* increased replicative life span, whereas CR failed to extend the replicative life span of a TOR1 mutant of budding yeast BY4742 (7). TOR inhibition by RNAi in *Caenorhabditis elegans* did not result in a further increase in the life span of the *eat-2* mutant, a CR mimetic strain (8). However, in *Drosophila melanogaster*, RM treatment further increased life span beyond the CR-mediated extension (9), suggesting that RM and CR affect life span, at least in part, via different mechanisms. Recently, mechanistic differences between RM and CR have been suggested

in rodents (10,11). Our recent studies using a budding yeast model also indicate that RM and CR may use different mechanisms to extend life span. We identified few significant changes in gene expression of CR associated with the TOR1 interaction (12). Furthermore, CR was found to extend the CLS of TOR1-deficient budding yeast BY4741 (12). Additionally, measurement of total reactive oxygen species (ROS) revealed that RM decreased ROS only in the exponential phase (2). In addition, we found that several mitochondrial parameters, including mitochondrial ROS, mitochondrial membrane potential, and ATP, were variably affected at different growth phases by RM and CR (2). Taken together, these data strongly imply that RM may not simply mimic the mechanistic pathways of CR.

Because the mechanistic difference between RM and CR is largely unknown, we first focused on the global effect of RM and CR by measuring transcriptome and metabolome expression to assess the unbiased effects of these two treatments. Then, we investigated main energy storage molecules including glycogen and lipid droplets (LDs).

Methods

Yeast Strain and Growth Conditions

Saccharomyces cerevisiae BY4741 was used as the wild-type strain. Isogenic single-gene deletion mutants and tandem affinity purification (TAP)-tagged strains (Supplementary Table 1) were grown in YPD media containing 2% glucose (control or non-caloric restriction [NR] conditions), 0.5% glucose (CR condition), or 2% glucose + 100 nM RM (RM condition). RM was purchased from Sigma. Yeast were grown at 30°C and 200 rpm as previously described (2).

Total RNA Extraction and Microarray

For RNA extraction, 20 OD_{600} units of yeast cells were harvested at day 5 and processed as previously described (12). Total RNA was further purified using the RNeasy Mini Kit (Qiagen) according to the manufacturer's instructions. To obtain gene expression profiles, we synthesized cRNA from 100 ng of total RNA by in vitro transcription for 16 hours using the GeneChip 3′ IVT PLUS Reagent Kit. The biotin-labeled cRNA was then hybridized onto an Affymetrix GeneChip Yeast 2.0 array (Affymetrix). Procedures following hybridization were the same as described in Choi and colleagues (12). Microarray experiments were conducted in biological triplicate for each condition.

Microarray Analysis

Microarray signals were normalized by robust multiarray average (RMA) using the Transcriptome Analysis Console 2.0 (TAC 2.0; Affymetrix). Principal component analysis (PCA) was performed using the R console (version 3.2.2; R Core Team, Austria). For the selection of differentially expressed genes (DEGs) between experimental conditions, we performed a one-way analysis of variance (ANOVA) following false discovery rate (FDR) adjustment using R. Pairwise comparisons using Tukey's Honestly Significant Difference (HSD) test with 95% confidence intervals were also performed with R. Enriched gene ontology (GO) terms for the selected DEGs were identified using GO Term Finder (version 0.83) and non-redundant GO terms were selected using REVIGO (13). The data reported in this publication have been deposited in NCBI's Gene Expression Omnibus and are accessible through the GEO Series accession number GSE82324.

CLS Assay

CLS experiments were performed by propidium iodide staining as previously described (12). Experimental details are provided in Supplementary Methods.

ATP, Glucose, and Acetic Acid Measurement

ATP, glucose, and acetic acid assays were carried out as described by Choi and colleagues (14) with minor modifications. Experimental details are provided in Supplementary Methods.

Glycogen Measurement

Two OD_{600} units of cells were harvested, washed in 1× phosphate-buffered saline (PBS), quickly frozen, and stored at −80°C prior to being used. Frozen cell pellets were resuspended in 250 µL of 0.25 M Na_2CO_3 and incubated at 95°C for 4 hours. Then, 150 µL of 1 M acetic acid and 600 µL of 0.2 M sodium acetate were added to each sample. Half of the extract was incubated overnight with 1.4 U of amyloglucosidase (Sigma). The reaction was then concentrated fivefold using a vacuum concentrator (N-Biotek, Korea) and glucose was measured using a glucose colorimetric assay kit (BioVision).

Flow Cytometry for LD Detection

Prepared cells (2 OD_{600} units) were washed in 1× PBS, resuspended in 1 mL of 4% paraformaldehyde solution, and stored at 4°C until use. For flow cytometric analysis of LDs, fixed cells were washed in 1× PBS and stained with 5 µg/mL BODIPY 493/503 (Invitrogen) at 30°C for 10 minutes (15). Next, cells were washed in 1× PBS and resuspended in 1 mL of 1× PBS. Fluorescence was measured with a flow cytometer (BD Biosciences).

Metabolite Extraction

Cells under NR (n = 6: control for CR and n = 6: control for RM), CR (n = 5), and RM (n = 4) conditions were harvested at day 5. Intracellular metabolites were collected through fast filtration (16). Briefly, 5 × 10^7 cells were collected by vacuum filtration through a 30-mm-diameter nylon membrane filter (0.45-µm pore size; Whatman) and washed with 1 mL of distilled water. Whole filters with cells were immediately mixed with 10 mL extraction solvent (acetonitrile:water mixture = 1:1, v/v) at −20°C and frozen in liquid nitrogen. The frozen extraction mixture was thawed on ice, vortexed for 3 minutes, and then centrifuged at 16,100g for 5 minutes at 4°C. The supernatants were then collected and dried using a speed vacuum concentrator (Labconco). Prior to gas chromatography/time-of-flight mass spectrometry (GC/TOF MS) analysis, the metabolite extract was derivatized with 5 µL of methoxyamine hydrochloride in pyridine (40 mg/mL; Sigma-Aldrich) for 90 minutes and 45 µL of *N*-methyl-*N*-trimethylsilyltrifluoroacetamide (Fluka, Switzerland) for 30 minutes at 37°C.

GC/TOF MS Analysis

An Agilent 7890B GC system (Agilent Technologies) equipped with a Pegasus HT TOF MS (LECO) was used for metabolite analysis. Derivatized samples were injected into the GC in splitless mode. Metabolites were separated in an RTX-5Sil MS column (30 m × 0.25 mm, 0.25-µm film thickness; Restek) and an additional 10-m long integrated guard column. Helium was used as the carrier gas with a flow rate of 1 mL/min. The temperature of the column oven was held at 50°C for 1 minutes, ramped to 330°C at 20°C/min, and held at 330°C for 5 minutes. The temperature of the ion source and

transfer line were maintained at 250°C and 280°C, respectively. Electron ionization was carried out at 70 eV and mass spectra were acquired at 10 spectra/s in a mass range of 85–500 *m/z*. GC/TOF MS data were preprocessed using LECO Chroma TOF software (version 4.50) for both detection of peaks and deconvolution of mass spectra, then further processed using BinBase, an in-house database, for identification of metabolites (17).

Analysis of Metabolome Data

A total of 113 metabolites were identified. We selected metabolites significantly changed under each condition (CR or RM), compared with their respective NR using an adjusted p-value < .01 and absolute value of $\log_2$ ratio > 1. p-Value was calculated and adjusted by Student's t test and FDR using R. Metabolite networks were analyzed based on known human metabolic networks using Cytoscape (version 3.2.1) and Metscape plug-in (version 3.1).

Measurement of Oxygen Consumption

The measurement was performed as described by Kwon and colleagues (18) with minor modification. Briefly, 10 OD_{600} units of yeast were placed into a closed 1-mL chamber to measure oxygen concentration using a Clark-type oxygen electrode (Oxygraph plus; Hansatech, UK) at 30°C following the manufacturer's instructions. Oxygen consumption rate was calculated using Oxygraph software.

Immunoblotting

Immunoblot assays were performed as previously described with minor modifications. The complete procedures are provided in Supplementary Methods.

Statistical Analysis

Unless otherwise noted, data are expressed as the mean ± *SEM* and statistical significance was assessed by Student's t test between NR and the other conditions.

Results

Despite Physiological Differences, Both CR and RM Maintained Intracellular ATP Levels With Aging

To measure physiological parameters, we used optimal conditions to maximize CLS for RM (100 nM) and CR (0.5% glucose) treatments as previously determined (2). Both RM and CR significantly increased CLS; however, the extent of life-span extension was much higher by RM treatment than CR (Figure 1A and Supplementary Figure 1).

RM-mediated cell cycle arrest has been identified (19). In addition, we observed growth retardation following RM treatment, and the retarded growth was restored to NR levels after 3 days (Figure 1B). CR did not alter growth during the exponential phase (Figure 1B). Consistent with entry into stationary phase (Figure 1B), media glucose was exhausted in order of CR, NR, and then RM (Figure 1C). Maximal acetate levels were 1.8, 1.5, and 5.2 mM under NR, CR, and RM conditions, respectively (Figure 1D). In addition, we measured media pH under the three conditions. Interestingly, pH abruptly increased to 7.5 when yeast entered stationary phase under CR, while with RM, it sharply dropped, fluctuated, and then remained at approximately 5. Under NR conditions, the pH gradually decreased to approximately 4.5 (Figure 1E).

Previously, we reported that under CR conditions, yeast maintained cellular ATP during the chronological aging process. To determine whether RM shows a similar tendency, we measured intracellular ATP levels through the chronological aging process (Figure 1F). Interestingly, cellular ATP levels were clearly maintained during the aging process under RM treatment (Figure 1F). In fact, RM maintained ATP almost to the same level as CR (Figure 1F).

Both CR and RM reduced ROS production (2). In addition, we observed increased oxygen consumption prior to entering stationary phases under CR (20 hours) and RM (69 hours) conditions (Figure 1G), which suggests enhanced mitochondrial capacity together with ATP production maintenance by CR and RM. Collectively, both RM and CR maintained cellular energy status during the chronological aging process.

CR Profoundly Altered Global Gene Expression Relative to RM

We next measured the alteration in global gene expression under CR and RM conditions to assess the unbiased characteristics of these two life-span extenders. We measured the transcriptome profiles on day 5, the time point at which intracellular ATP maximally changed (Figure 1F), but life span and growth were not affected (Figure 1A and B). The global gene expression data of the three conditions are displayed as distinct clusters on a two-dimensional PCA plot (Figure 2A). Next, we determined the number of DEGs under CR and RM conditions. DEGs were defined as genes that exhibited both p-value < .05 and absolute fold-change (FC) > 2 between the treatment and control. All DEGs are listed in Supplementary Table 2.

Transcriptome alteration was more prominent in CR than in RM, as shown in the volcano plots (Supplementary Figure 2). A comparison between CR and RM also showed that CR had a stronger effect than RM (Supplementary Figure 2). CR upregulated and downregulated 1,003 and 1,083 DEGs, respectively, whereas RM upregulated 219 and downregulated 220 genes. Interestingly, a comparison of the whole CR and RM transcriptomes showed a change of approximately 25% (1,421 genes) using identical statistical criteria for DEG selection (Supplementary Figure 2). Of these, 712 genes were upregulated and 709 genes were downregulated in CR versus RM.

We further compared the overlap of the selected DEGs using a Venn diagram (Figure 2B and C). The size of the circles emphasized the greater impact of CR compared with that of RM. RM-related DEGs (RM vs control) overlapped substantially with CR-related DEGs (CR vs control); 42% of the upregulated DEGs (92 out of 219 genes) and 81% of the downregulated DEGs (179 out of 220 genes) overlapped with CR-related DEGs. The Venn diagram also showed significantly distinct CR-related DEGs (91% of upregulated DEGs and 83% of downregulated DEGs) compared with RM-related DEGs. Interestingly, the genes changed by CR versus control largely overlapped (approximately 80%) with the genes changed by CR versus RM.

CR- and RM-Related DEGs Were Associated With Different Biological Processes and Cellular Components

In order to identify biological process and cellular component terms significantly affected by CR and RM, we analyzed enrichment of GO using GO Term Finder. The complete results of the GO term analysis are provided in Supplementary Tables 3 and 4. The DEGs upregulated by CR versus control showed enriched biological process terms related to transcription, proteasome-ubiquitin–mediated protein degradation, proteasome- and ubiquitin-dependent regulation of anaphase-promoting complex,

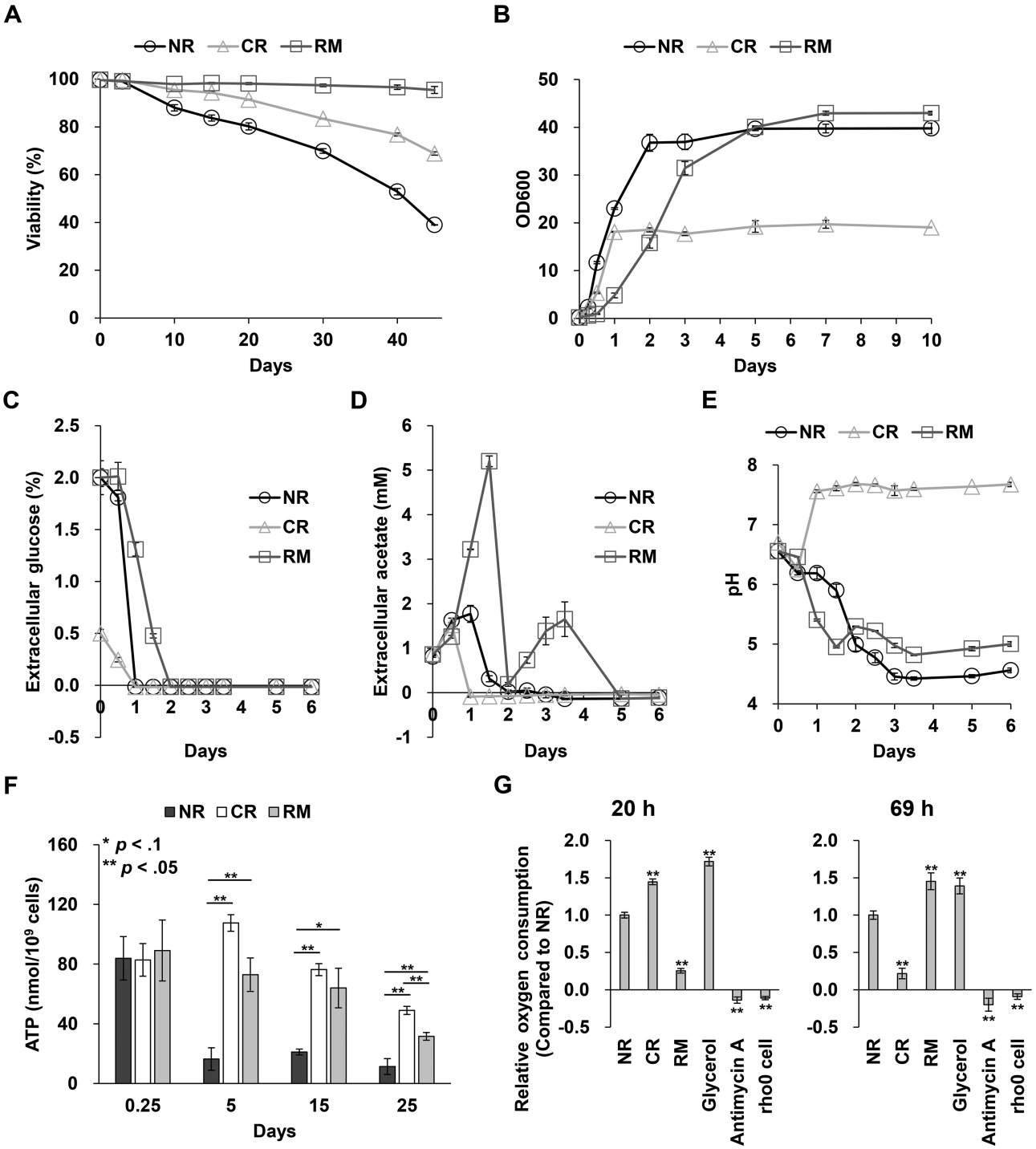

Figure 1. Both caloric restriction (CR) and rapamycin (RM) extend chronological life span (CLS) and maintain ATP levels throughout the chronological aging process. **(A)** CLS under non-caloric restriction (NR), CR, and RM treatment. **(B)** Growth curves under the three conditions. **(C)** Changes in media glucose levels. **(D)** Production of acetate in media. **(E)** Changes in media pH. **(F)** ATP levels under the three conditions during the chronological aging process. **(G)** Oxygen consumption rates at 20 and 69 hours under NR, CR, and RM conditions (NR was set to 1). Glycerol (2%) was used as a positive control and antimycin A (50 μM) and rho^0 cells were used as negative controls. *$p < .1$ and **$p < .05$.

autophagy including mitophagy, microtubule polymerization, chromosome segregation, cell cycle regulation, and cellular metal ion homeostasis, especially iron (Figure 2D). Consistent with these terms, autophagosome, peroxisome, ubiquitin ligase complex, and chromosome kinetochore were selected as significantly enriched cellular component terms under CR conditions (Supplementary Table 3). Interestingly, GO Term Finder did not find any enriched biological process terms among the DEGs upregulated by RM versus control. However, cell wall and membrane were found as significant cellular component terms using the DEGs upregulated by RM (Supplementary Table 3). In addition, we analyzed the DEGs from the comparison between CR and RM for enriched

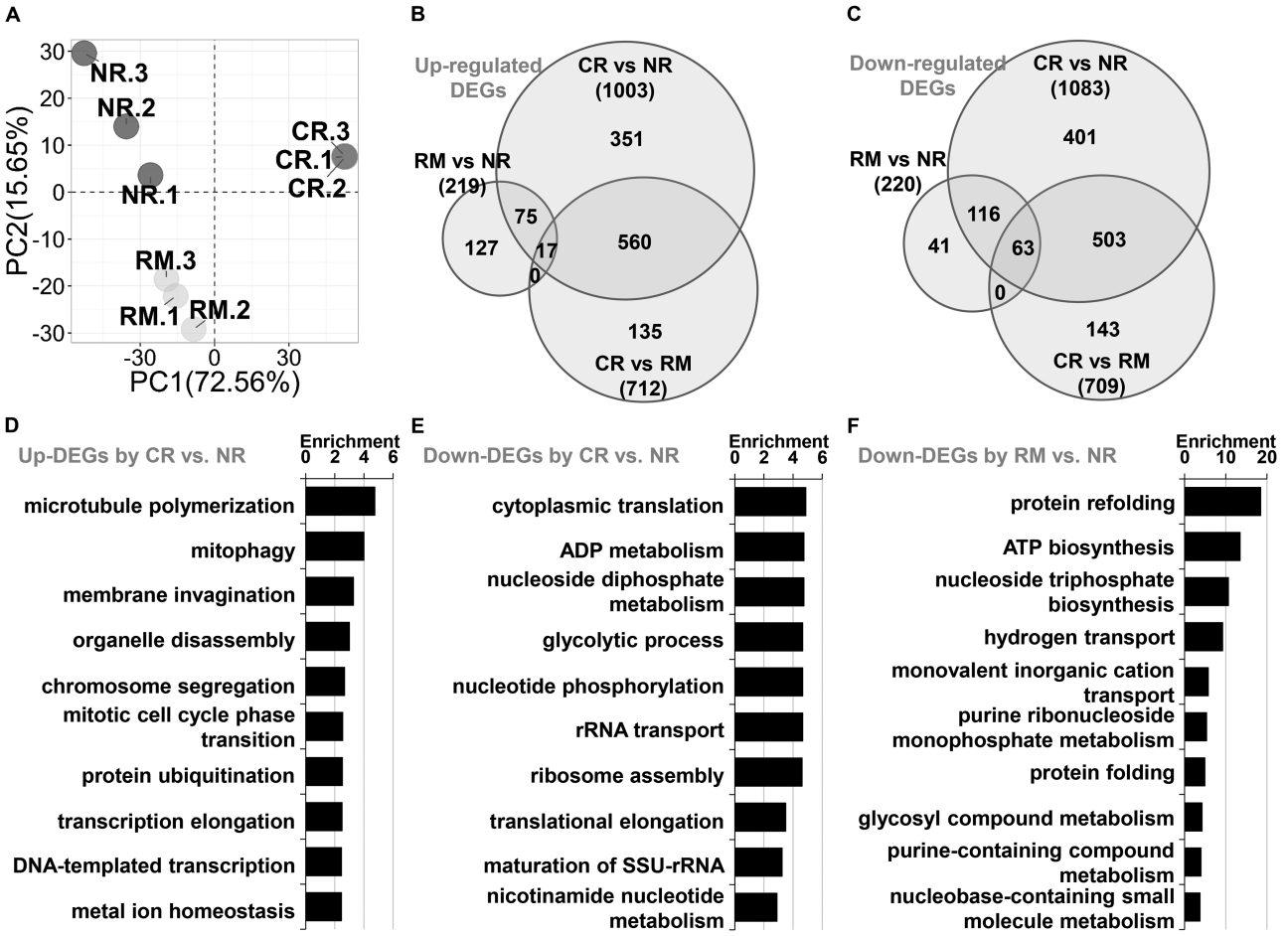

Figure 2. Global gene expression profiles show mechanistic differences between caloric restriction (CR) and rapamycin (RM) treatment conditions. **(A)** Principal component analysis (PCA) using the transcriptome profiles of non-caloric restriction (NR), CR, and RM treatment. Approximately 90% of the variability in the data set is captured by two principal components. **(B** and **C)** Proportional Venn diagrams show the number of upregulated differentially expressed gene (DEGs) **(B)** and downregulated DEGs **(C)** in the three comparisons. **(D** to **F)** Bar plots show nonredundant enriched biological process terms in DEGs upregulated by CR versus NR. **(D)** DEGs downregulated by CR versus NR. **(E)** DEGs downregulated by RM versus NR. **(F)** Selected biological process terms sorted by enrichment scores (x-axis). A complete list of biological process terms is provided in Supplementary Tables 3 and 4.

GO terms. Interestingly, we identified similar terms selected for CR versus control including transcription, proteolysis, autophagy, microtubule polymerization, chromosome segregation, and negative regulation of cell cycle using the upregulated DEGs. However, we also identified additional biological process terms including DNA conformational change and response to unfolded protein, and cellular protein complex assembly including proteasome, microtubule, and electron transport chain (Supplementary Table 3). Similar to these terms, the cellular component terms included proteasome complex, histone acetyltransferase complex, kinetochore, RNA polymerase II transcription factor complex, and microtubule cytoskeleton.

Analysis of the CR versus control downregulated DEGs identified small molecule metabolism, including glycolytic metabolites, nucleic acid metabolites, and cofactors; translation, including ribosome components and rRNA components; and regulation of translational elongation as enriched biological process terms (Figure 2E). Interestingly, most of these biological process terms were also enriched in the analysis of CR versus RM downregulated genes (Supplementary Table 4). RM versus NR downregulated DEGs showed enrichment of biological process terms associated with protein folding and ATP biosynthesis (Figure 2F).

Several Amino Acids Were Increased Under CR, But Not Under RM

To characterize metabolic differences between CR and RM treatments, we applied a metabolomics approach (16). We successfully detected 113 metabolites simultaneously and applied rigorous statistical criteria including FDR-adjusted p-value < .01 and absolute FC > 2 for the selection of significantly changed metabolites. The complete metabolomics results are provided in Supplementary Table 5.

All detected metabolites under CR and RM conditions were analyzed using MetScape and depicted as metabolic networks, except for metabolites that are not in the network database. CR significantly changed 39 metabolites (34.5%); 27 metabolites increased and 12 decreased (Figure 3). We found that amino acids, mostly standard amino acids used in proteins, were the predominant metabolites increased by CR, notably two branched-chain amino acids (BCAAs), leucine (FC = 3.3) and valine (FC = 2.3). Interestingly, several genes responsible for de novo biosynthesis of BCAAs, including *BAT1*, *ILV2*, *ILV3*, and *ILV5* (Supplementary Table 2), were consistently downregulated by CR, which may suggest that the increase of intracellular BCAAs is not a result of de novo biosynthesis, but rather salvage from autophagy-mediated degradation.

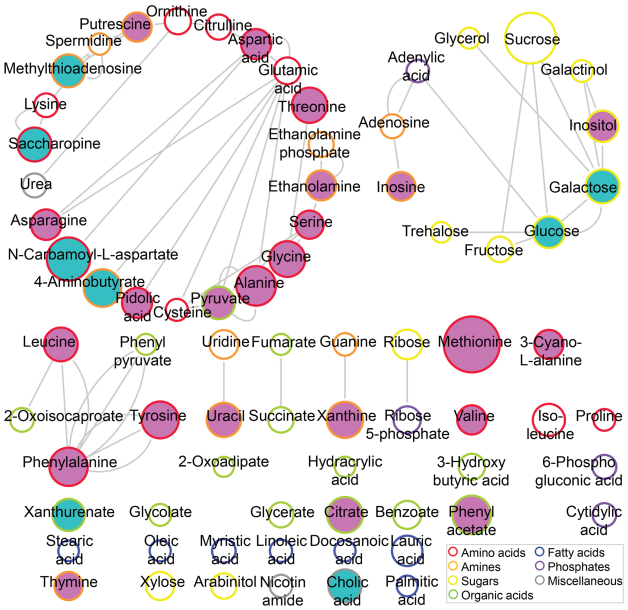

Figure 3. Caloric restriction (CR) increases free amino acids. Metabolome profile of intracellular metabolites altered by CR. Node and edge indicate metabolite and chemical association, respectively. Node size is correlated with the absolute value of the $\log_2$ ratio of CR/NR. Significantly changed metabolites are indicated by pink-filled symbols (upregulated metabolites) or green-filled symbols (downregulated metabolites). The border color of nodes indicates metabolite types listed in the gray box. The complete metabolite list of the metabolome data is detailed in Supplementary Table 5. NR = non-caloric restriction.

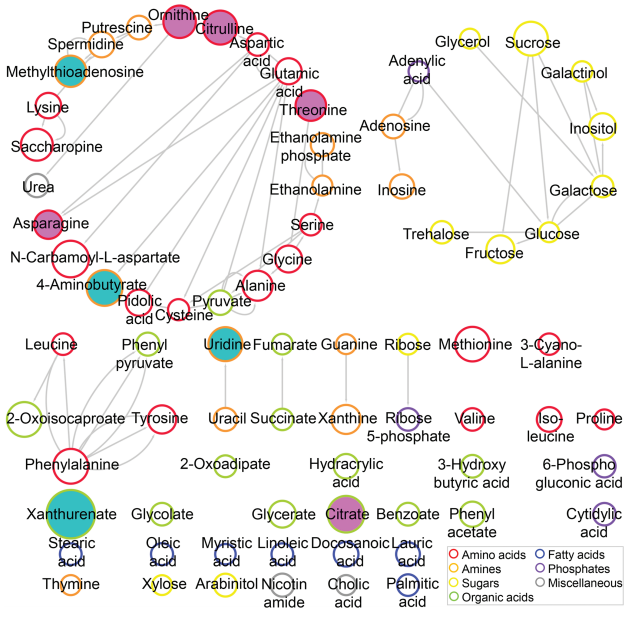

Figure 4. Rapamycin (RM) has little effect on the metabolome. Metabolome profile of intracellular metabolites altered by RM. Node and edge indicate metabolite and chemical association, respectively. Node size is correlated with the absolute value of the $\log_2$ ratio of RM/NR. Significantly changed metabolites are indicated by pink-filled symbols (upregulated metabolites) or green-filled symbols (downregulated metabolites). The border color of nodes indicates metabolite types listed in the gray box. The complete metabolite list of the metabolome data is detailed in Supplementary Table 5. NR = non-caloric restriction.

RM significantly changed 12 metabolites (10.6%); six metabolites increased and six decreased (Figure 4). Four metabolites were specifically altered by only by RM treatment including citrulline (FC = 3.4), ornithine (FC = 3.0), homoserine (unmapped in MetScape database; FC = 2.2), and uridine (FC = −3.4) (Figure 4). RM had less of an impact on amino acids, except for asparagine and threonine.

CR Repressed Genes for Carbohydrate Metabolism and Activated Genes for Lipid Metabolism

Because both CR and RM primarily influence energy metabolism, we analyzed transcriptome and metabolome profiles related to carbohydrate and lipid metabolism. We found that CR strongly suppressed genes responsible for major energy pathways including glycolysis, the tricarboxylic acid (TCA) cycle, and oxidative phosphorylation, as well as other branch pathways such as glycogen metabolism and the pentose-phosphate shunt (Supplementary Figure 3). We also observed that RM had less of an impact on these genes. Interestingly, both CR and RM significantly suppressed genes responsible for the ATP synthase complex of the electron transport chain. CR specifically decreased glucose and malate metabolites and increased pyruvate metabolite (Supplementary Figure 3). Citrate was increased by both CR and RM. Collectively, these data indicate that CR and RM have sufficient energy sources to maintain ATP levels, regardless of transcriptional gene repression of energy pathways.

Regarding lipid metabolism, CR strongly repressed genes responsible for ergosterol biosynthesis and the glyoxylate cycle (Supplementary Figure 4). RM also repressed genes responsible for ergosterol biosynthesis, but less effectively than CR; however, RM showed little effect on genes responsible for the glyoxylate cycle (Supplementary Figure 4).

Interestingly, CR increased the mRNA levels of several genes required for the formation of triacylglycerol (*DGA1*), formation of steryl ester (*ARE2*), catabolism of triacylglycerol (*TGL3* and *TGL4*), and activation of long-chain fatty acid (*FAA4*) (Supplementary Figure 4). These results indicate that CR might activate β-oxidation. Indeed, we found that *OAF1*, a positive regulator of β-oxidation, was upregulated by CR, but not by RM (Supplementary Table 2). In addition, *SNF1*, which encodes a protein kinase that positively regulates another β-oxidation activator, ADR1p, was upregulated by CR (Supplementary Table 2). Furthermore, we tested the importance of fatty acid β-oxidation by targeting a few critical genes encoding enzymes involved in this pathway including *POX1* (a fatty-acyl coenzyme A oxidase) and *FOX2* (an enoyl-CoA hydratase and a 3-hydroxyacyl-CoA dehydrogenase). CR failed to increase the life span of *pox1Δ* and *fox2Δ* strains, whereas RM successfully increased their life span (Supplementary Figure 8).

CR and RM Differently Affected Major Energy Storage Molecules

Because major metabolism genes were significantly altered by CR, but not by RM in our global gene expression analysis, we measured major energy storage molecules under both treatments. First, we measured changes in glycogen levels. We used mutants lacking genes encoding enzymes involved in glycogen synthesis (either GSY2 or GLC3) or breakdown (GDB1) as positive and negative controls, respectively. As expected, *gdb1Δ* showed high glycogen levels, whereas *gsy2Δ* and *glc3Δ* showed low glycogen levels (Figure 5A). CR dramatically reduced glycogen accumulation after entering the stationary phase (Figure 5A). In contrast, glycogen levels were not altered by RM (Figure 5A).

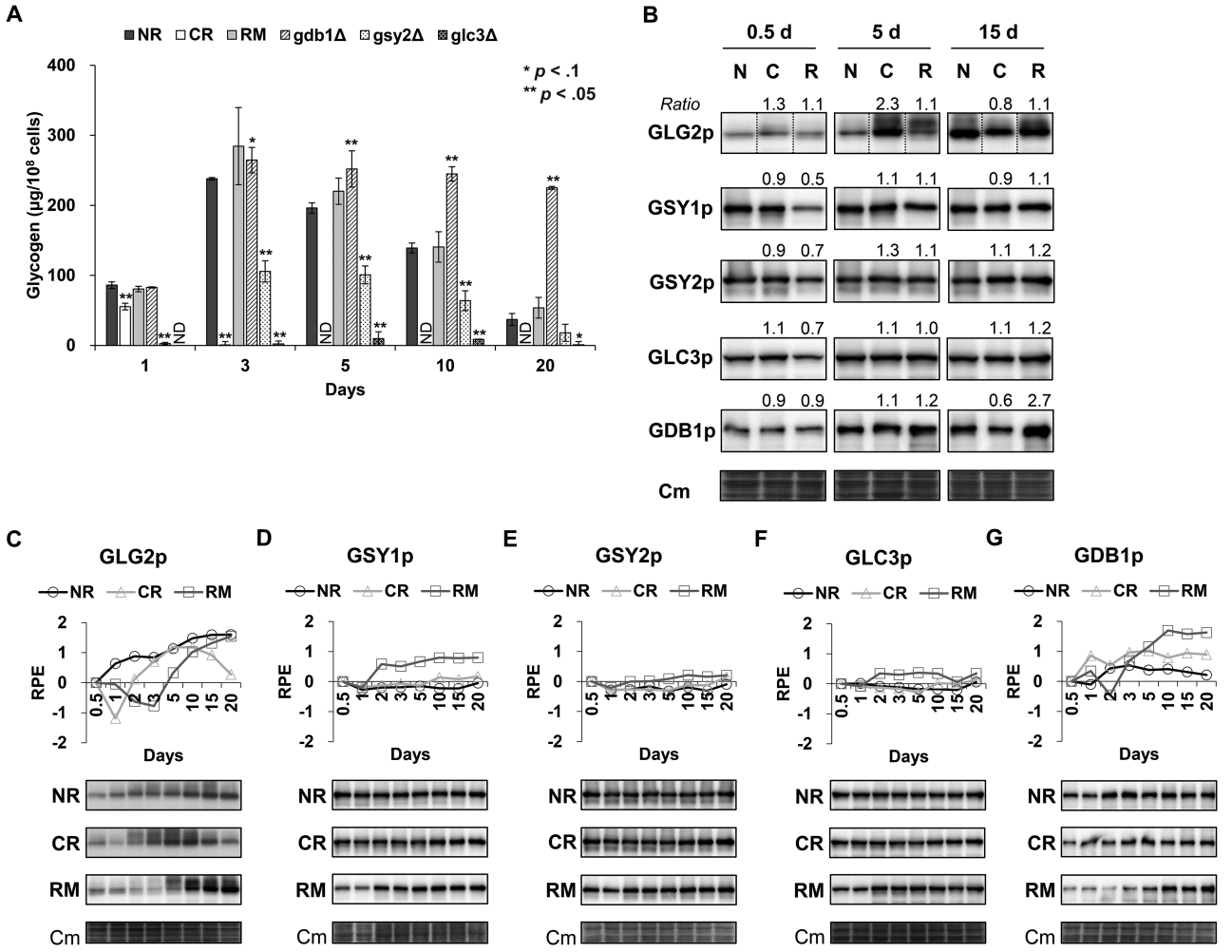

Figure 5. Glycogen is severely decreased by caloric restriction (CR), but maintained by rapamycin (RM). The expression of proteins involved in glycogen breakdown is increased by RM during the late stage of the chronological aging process. **(A)** Glycogen amount was measured in whole cell extracts under non-caloric restriction (NR), CR, and RM conditions throughout the chronological aging process. Single-gene deletion mutants with higher (*gdb1*Δ) or lower glycogen levels (*gsy2*Δ and *glc3*Δ) compared with that of wild type were used as positive and negative controls, respectively. ND: not detected. $*p < .1$ and $**p < .05$ relative to NR. **(B)** Proteins required for glycogen biosynthesis (GLG2, GSY1, GSY2, and GLC3) and degradation (GDB1) were detected under NR (N in image), CR (C), and RM (R) conditions at 0.5, 5, and 15 days. Immunoblot ratios between CR and NR (C/N) or between RM and NR (R/N) are presented. Cm: Coomassie blue stain. **(C** to **G)** Protein levels of GLG2p **(C)**, GSY1p **(D)**, GSY2p **(E)**, GLC3p **(F)**, and GDB1p **(G)** were measured under NR, CR, and RM conditions during the chronological aging process. Relative protein expression (RPE) at the indicated time points was normalized to the signal at day 0.5. Log-transformed ratios were used for graphs (y-axis).

In addition, we quantified proteins responsible for glycogen biosynthesis (GLG2p, GSY1p, GSY2p, and GLC3p) and breakdown (GDB1p) at day 0.5, 5, and 15 (Figure 5B) comparing CR and RM with the control. A marked increase in GLG2p at day 5 and a decrease at day 15 were detected under CR conditions. GDB1p was clearly decreased at day 15 by CR; however, it was increased at day 15 by RM. In addition, we monitored the expression of these proteins throughout the chronological aging process. We found that GLG2p gradually increased under control conditions; however, RM suppressed the increase and recovered levels by day 20 (Figure 5C). Interestingly, the protein levels were highest at day 10 under CR conditions and sharply decreased afterwards. GSY1p, GSY2p, and GLC3p were unchanged under both control and CR conditions; however, there levels increased at day 2 and were subsequently maintained under RM conditions (Figure 5D–F). GDB1p increased at day 2 under control conditions, at day 1 under CR conditions, and at day 3 under RM conditions (Figure 5G). GDB1p levels were subsequently maintained in all conditions. Overall, these data imply that similar quantities of glycogen are stored under RM and NR conditions; however, under RM, glycogen might be utilized more effectively because of increases in enzymes involved in glycogen breakdown.

In addition, we measured LD levels under the three conditions during the chronological aging process (Figure 6). LDs were increased at day 3 and were maintained during the chronological aging process under NR conditions (Figure 6A). CR decreased and maintained LDs at an approximately threefold lower level than NR during the chronological aging process. However, RM slightly decreased LDs, exhibiting a bell-shaped pattern. We also analyzed the distribution of BODIPY-stained cells and found the same single peak in both CR and RM conditions compared with multiple peaks under NR conditions (Supplementary Figure 5A). Microscopic images clearly showed different sizes of LDs under the three conditions; the smallest under CR conditions and similar sizes under RM and NR conditions (Supplementary Figure 5B).

In addition, we measured protein levels involved in LD biosynthesis (DGA1p and the two human orthologs SCS3p and YFT2p)

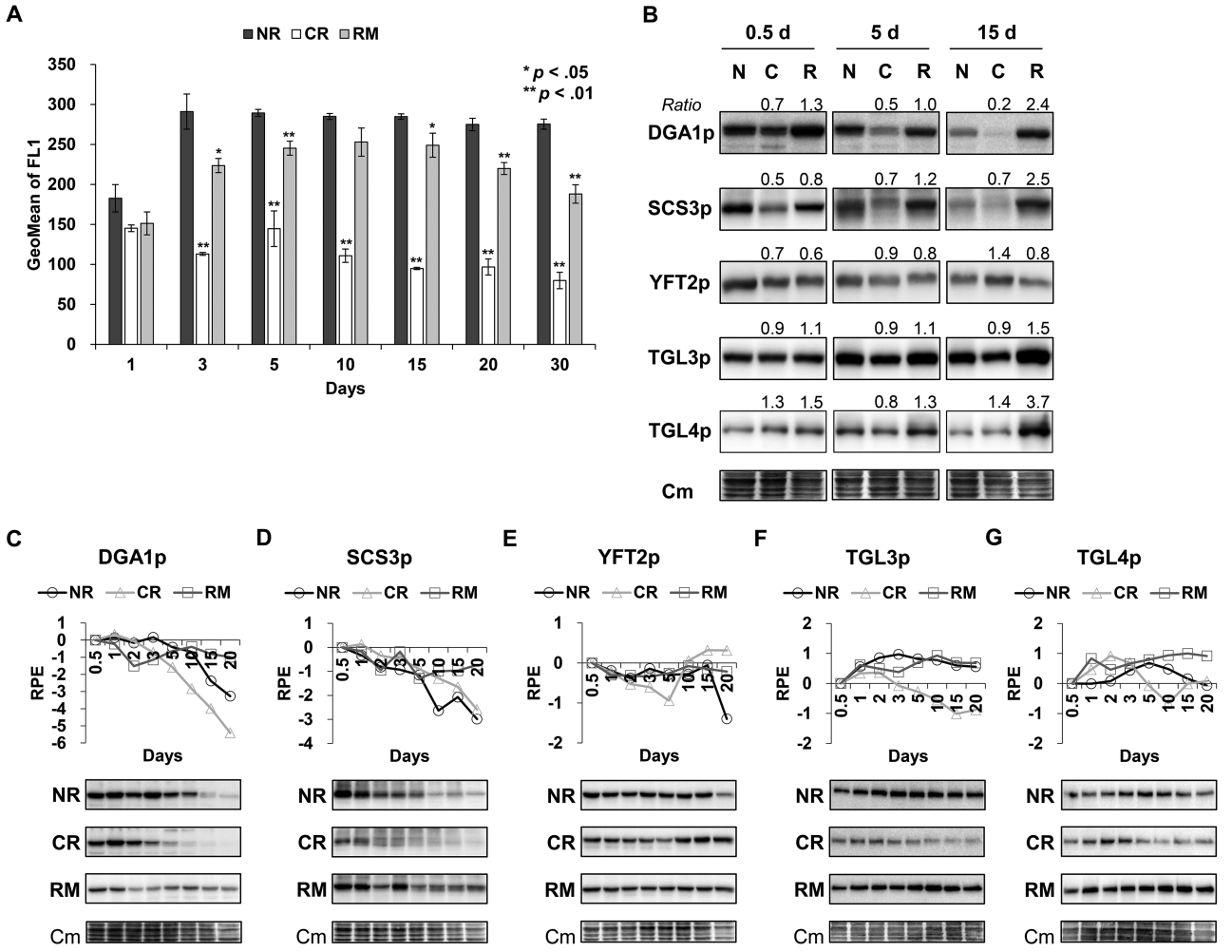

Figure 6. Lipid droplets (LDs) are severely reduced by caloric restriction (CR), but only slightly reduced by rapamycin (RM). The expression of proteins involved in lipid degradation is increased by RM at the late stage of the chronological aging process. Cells were harvested during the chronological aging process and stained with neutral lipid-specific BODIPY 493/503. Fluorescent signals were measured using flow cytometry. **(A)** Bar graph (mean ± *SEM*) of the signals under non-caloric restriction (NR), CR, and RM conditions. **(B)** Expression level of proteins responsible for neutral lipid synthesis (DGA1p, SCS3p, and YFT2p) and degradation (TGL3p and TGL4p) under NR (N), CR (C), and RM (R) conditions at 0.5, 5, and 15 days. Immunoblot ratios between CR and NR (C/N) or between RM and NR (R/N) are presented. Cm: Coomassie blue stain. **(C** to **G)** Protein levels of DGA1p **(C)**, SCS3p **(D)**, YFT2p **(E)**, TGL3p **(F)**, and TGL4p **(G)** under NR, CR, and RM conditions during the chronological aging process. Relative protein expression (RPE) at the indicated time points was normalized to the signal at day 0.5. Log-transformed ratios were used for graphs (y-axis).

and TAG degradation (TGL3p and TGL4p; Figure 6B). Comparing the three conditions, DGA1p, SCS3p, and TGL3p were decreased under CR conditions; however, they were increased under RM conditions, including TGL4p (Figure 6B). We further measured these proteins throughout the chronological aging process. DGA1p and SCS3p gradually decreased under both NR and CR conditions; however, they were maintained under RM conditions (Figure 6C and D). YFT2p levels were maintained up to day 15 under both NR and RM conditions; however, they were decreased up to day 5 and then increased under CR conditions (Figure 6E). TGL3p levels initially increased and were subsequently maintained under both NR and RM conditions; however, TGL3p levels decreased under CR conditions (Figure 6F). TGL4p showed the most complex patterns (Figure 6G); protein levels gradually increased and then decreased under NR conditions. A similar, but more rapid, pattern was observed under CR conditions, while under RM conditions, TGL4p increased at day 1 and was maintained subsequently.

Taken together, these results indicate that RM activates LD biosynthesis, while simultaneously promoting LD degradation. This suggests that RM might maintain cellular energy levels via effective breakdown of LDs.

Discussion

The intriguing observation that RM extends life span without dietary restrictions has spurred interest in understanding its underlying molecular mechanisms. In this study, we observed a limited response in our yeast model under RM versus CR conditions in terms of transcriptome and metabolome, as well as energy storage molecules including glycogen and LDs. Our findings are consistent with those of recent studies in mice, which showed that CR, but not RM, induced extensive changes in transcriptome (11,20) and metabolome (20). CR also demonstrated significant inhibition of adiposity (10,21,22) and activation of β-oxidation (10); however,

these phenotypes were not observed under RM conditions. Mouse studies further showed the different impact of these two regimens on endocrine status (21,23), glutathione level (21), and proteome dynamics (24,25). However, similar to the omics data, while CR had an extensive influence on these parameters, RM had little effect. Taken together, these studies strongly suggest that RM has an overlapping mechanism similar to CR, as well as a distinct mechanism dissimilar to that of CR.

RM resulted in significantly fewer changes in global transcriptome and metabolome compared with CR, in spite of the extraordinary increase of life span demonstrated in our study. Next, we attempted to analyze the occurrences in RM-treated yeast cells. RM produced higher levels of extracellular acetate (Figure 1D) and media pH fluctuation (Figure 1E) compared with NR and CR conditions. Although the connection between acetate and pH levels and RM-induced longevity is unclear at this point, we hypothesize that RM has a metabolic status different from that of CR. RM increased oxygen consumption (Figure 1G) and reduced ROS (2), which might contribute to enhanced mitochondrial capacity. Improved mitochondrial capacity may aid in maintaining ATP levels and consequently extending life span (26). Furthermore, RM increased the protein expression of enzymes involved in glycogen and LD breakdown, including GDB1p (Figure 5B) and TGL4p (Figure 6B), at a late stage of the chronological aging process (day 15) compared with NR. Increased levels of these enzymes might be useful for mobilizing major energy storage molecules to maintain ATP levels until late stages of the chronological aging process.

Despite the possible roles of RM in TORC1-downstream processes, including inhibition of translation and ribosome biogenesis, and activation of autophagy, no related GO terms were found at day 5 (Figure 2F and Supplementary Figure 6). Hardwick and colleagues obtained microarray data at early time points following treatment of budding yeast with 100 nM of RM; they identified most of the well-known TORC1-downstream processes within 2 hours post RM treatment (27) (Supplementary Figure 7). Therefore, the phenotypes caused by RM inhibition of TORC1 could constitute early responses; however, they are not maintained during cellular longevity.

CR increased the mRNA levels of several genes required for triacylglycerol formation (DGA1) and triacylglycerol catabolism (TGL3) (Supplementary Figure 4); however, their protein levels were decreased (Figure 6B). In general, although mRNA is translated into protein, there is a poor correlation between mRNA and protein levels globally (28). This suggests the existence of complicated mRNA-protein discoupling mechanisms such as additional levels of regulation including mRNA stability, ribosomal occupancy, and protein half-life. Interestingly, translation was an enriched GO term among the DEGs downregulated by CR; this might partially explain the discrepancy between the mRNA and protein levels of DGA1 and TGL3.

Previously, we found a longevity-related gene set that was altered by CR during the transition from exponential to stationary growth (12). The gene set contained 646 genes, a majority of which (60%: 375 genes) overlapped with CR DEGs identified in this study. These overlapping genes showed enriched terms involved in two biological pathways, glycolysis and ATP metabolism. These results emphasize that transcriptional repression of genes responsible for energy metabolism is an important modification in obtaining cellular longevity by CR.

Recent reviews have emphasized two roles of autophagy in cellular longevity, cytoprotection and bioenergetics (29). Our GO term analysis using DEGs upregulated by CR also revealed autophagy as an enriched biological process term (Supplementary Table 3). Consistent with the transcriptional activation of autophagy, we also observed an increase in intracellular amino acids, including BCAAs in our metabolomics data (Figure 3). Interestingly, it has been reported that BCAA supplement increases life span in yeast (30,31), as well as in higher organisms (32,33). Overall, our data indicate that activation of genes involved in autophagy and increase of BCAAs might contribute to cellular longevity by CR.

In conclusion, RM induces relatively few changes in the global transcriptome and metabolome compared with CR. In particular, CR upregulated genes responsible for autophagy and β-oxidation and increased various intracellular amino acids. A noteworthy difference between the CR and RM treatments was their influence on storage molecules. CR dramatically reduced the accumulation of glycogen and LDs; however, RM did not change or had little effect on the amount of these molecules. RM increased the protein expression of enzymes responsible for the degradation of energy storage molecules, which might lead to efficient utilization of glycogen and LDs during the chronological aging process. Altogether, although both CR and RM lead to longevity by securing cellular energy, our data indicate that they do so through distinct mechanisms.

Supplementary Material

Supplementary data is available at *The Journals of Gerontology, Series A: Biomedical Sciences and Medical Sciences* online.

Funding

This work was carried out with the support of Cooperative Research Program for the Agriculture Science & Technology Development (Project No. PJ01195001), Rural Development Administration, Republic of Korea and Bio and Medical Technology Development Program through the National Research Foundation of Korea funded by the Ministry of Education, Science and Technology (NRF 2015M3A9B4071075).

Conflict of Interest

The authors confirm that no conflicts of interest exist.

References

1. Fontana L, Partridge L, Longo VD. Extending healthy life span–from yeast to humans. *Science*. 2010;328:321–326. doi:10.1126/science.1172539
2. Choi KM, Lee HL, Kwon YY, Kang MS, Lee SK, Lee CK. Enhancement of mitochondrial function correlates with the extension of lifespan by caloric restriction and caloric restriction mimetics in yeast. *Biochem Biophys Res Commun*. 2013;441:236–242. doi:10.1016/j.bbrc.2013.10.049
3. Arriola Apelo SI, Pumper CP, Baar EL, Cummings NE, Lamming DW. Intermittent administration of rapamycin extends the life span of female C57BL/6J mice. *J Gerontol A Biol Sci Med Sci*. 2016;71:876–881. doi:10.1093/gerona/glw064
4. Loewith R, Jacinto E, Wullschleger S, et al. Two TOR complexes, only one of which is rapamycin sensitive, have distinct roles in cell growth control. *Mol Cell*. 2002;10:457–468. doi:10.1016/S1097-2765(02)00636-6
5. Arriola Apelo SI, Lamming DW. Rapamycin: an InhibiTOR of aging emerges from the soil of Easter Island. *J Gerontol A Biol Sci Med Sci*. 2016;71:841–849. doi:10.1093/gerona/glw090
6. Lamming DW, Ye L, Katajisto P, et al. Rapamycin-induced insulin resistance is mediated by mTORC2 loss and uncoupled from longevity. *Science*. 2012;335:1638–1643. doi:10.1126/science.1215135

7. Kaeberlein M, Powers RW 3rd, Steffen KK, et al. Regulation of yeast replicative life span by TOR and Sch9 in response to nutrients. *Science*. 2005;310:1193–1196. doi:10.1126/science.1115535
8. Hansen M, Chandra A, Mitic LL, Onken B, Driscoll M, Kenyon C. A role for autophagy in the extension of lifespan by dietary restriction in *C. elegans*. *PLoS Genet*. 2008;4:e24. doi:10.1371/journal.pgen.0040024
9. Bjedov I, Toivonen JM, Kerr F, et al. Mechanisms of life span extension by rapamycin in the fruit fly *Drosophila melanogaster*. *Cell Metab*. 2010;11:35–46. doi:10.1016/j.cmet.2009.11.010
10. Yu Z, Wang R, Fok WC, Coles A, Salmon AB, Pérez VI. Rapamycin and dietary restriction induce metabolically distinctive changes in mouse liver. *J Gerontol A Biol Sci Med Sci*. 2015;70:410–420. doi:10.1093/gerona/glu053
11. Fok WC, Livi C, Bokov A, et al. Short-term rapamycin treatment in mice has few effects on the transcriptome of white adipose tissue compared to dietary restriction. *Mech Ageing Dev*. 2014;140:23–29. doi:10.1016/j.mad.2014.07.004
12. Choi KM, Kwon YY, Lee CK. Characterization of global gene expression during assurance of lifespan extension by caloric restriction in budding yeast. *Exp Gerontol*. 2013;48:1455–1468. doi:10.1016/j.exger.2013.10.001
13. Supek F, Bošnjak M, Škunca N, Šmuc T. REVIGO summarizes and visualizes long lists of gene ontology terms. *PLoS One*. 2011;6:e21800. doi:10.1371/journal.pone.0021800
14. Choi KM, Kwon YY, Lee CK. Disruption of Snf3/Rgt2 glucose sensors decreases lifespan and caloric restriction effectiveness through Mth1/Std1 by adjusting mitochondrial efficiency in yeast. *FEBS Lett*. 2015;589:349–357. doi:10.1016/j.febslet.2014.12.020
15. Radulovic M, Knittelfelder O, Cristobal-Sarramian A, Kolb D, Wolinski H, Kohlwein SD. The emergence of lipid droplets in yeast: current status and experimental approaches. *Curr Genet*. 2013;59:231–242. doi:10.1007/s00294-013-0407-9
16. Kim S, Lee DY, Wohlgemuth G, Park HS, Fiehn O, Kim KH. Evaluation and optimization of metabolome sample preparation methods for *Saccharomyces cerevisiae*. *Anal Chem*. 2013;85:2169–2176. doi:10.1021/ac302881e
17. Lee DY, Fiehn O. High quality metabolomic data for Chlamydomonas reinhardtii. *Plant Methods*. 2008;4:7. doi:10.1186/1746-4811-4-7
18. Kwon YY, Choi KM, Cho C, Lee CK. Mitochondrial efficiency-dependent viability of *Saccharomyces cerevisiae* mutants carrying individual electron transport chain component deletions. *Mol Cells*. 2015;38:1054–1063. doi:10.14348/molcells.2015.0153
19. Heitman J, Movva NR, Hall MN. Targets for cell cycle arrest by the immunosuppressant rapamycin in yeast. *Science*. 1991;253:905–909. doi:10.1126/science.1715094
20. Fok WC, Bokov A, Gelfond J, et al. Combined treatment of rapamycin and dietary restriction has a larger effect on the transcriptome and metabolome of liver. *Aging Cell*. 2014;13:311–319. doi:10.1111/acel.12175
21. Fok WC, Zhang Y, Salmon AB, et al. Short-term treatment with rapamycin and dietary restriction have overlapping and distinctive effects in young mice. *J Gerontol A Biol Sci Med Sci*. 2013;68:108–116. doi:10.1093/gerona/gls127
22. Carter CS, Khamiss D, Matheny M, et al. Rapamycin versus intermittent feeding: dissociable effects on physiological and behavioral outcomes when initiated early and late in life. *J Gerontol A Biol Sci Med Sci*. 2016;71:866–875. doi:10.1093/gerona/glu238
23. Miller RA, Harrison DE, Astle CM, et al. Rapamycin-mediated lifespan increase in mice is dose and sex dependent and metabolically distinct from dietary restriction. *Aging Cell*. 2014;13:468–477. doi:10.1111/acel.12194
24. Dai DF, Karunadharma PP, Chiao YA, et al. Altered proteome turnover and remodeling by short-term caloric restriction or rapamycin rejuvenate the aging heart. *Aging Cell*. 2014;13:529–539. doi:10.1111/acel.12203
25. Karunadharma PP, Basisty N, Dai DF, et al. Subacute calorie restriction and rapamycin discordantly alter mouse liver proteome homeostasis and reverse aging effects. *Aging Cell*. 2015;14:547–557. doi:10.1111/acel.12317
26. Guarente L. Mitochondria–a nexus for aging, calorie restriction, and sirtuins? *Cell*. 2008;132:171–176. doi:10.1016/j.cell.2008.01.007
27. Hardwick JS, Kuruvilla FG, Tong JK, Shamji AF, Schreiber SL. Rapamycin-modulated transcription defines the subset of nutrient-sensitive signaling pathways directly controlled by the Tor proteins. *Proc Natl Acad Sci U S A*. 1999;96:14866–14870. doi:10.1073/pnas.96.26.14866
28. Greenbaum D, Colangelo C, Williams K, Gerstein M. Comparing protein abundance and mRNA expression levels on a genomic scale. *Genome Biol*. 2003;4:117. doi:10.1186/gb-2003-4-9-117
29. Madeo F, Tavernarakis N, Kroemer G. Can autophagy promote longevity? *Nat Cell Biol*. 2010;12:842–846. doi:10.1038/ncb0910-842
30. Alvers AL, Fishwick LK, Wood MS, et al. Autophagy and amino acid homeostasis are required for chronological longevity in *Saccharomyces cerevisiae*. *Aging Cell*. 2009;8:353–369. doi:10.1111/j.1474-9726.2009.00469.x
31. Aris JP, Alvers AL, Ferraiuolo RA, et al. Autophagy and leucine promote chronological longevity and respiration proficiency during calorie restriction in yeast. *Exp Gerontol*. 2013;48:1107–1119. doi:10.1016/j.exger.2013.01.006
32. Mansfeld J, Urban N, Priebe S, et al. Branched-chain amino acid catabolism is a conserved regulator of physiological ageing. *Nat Commun*. 2015;6:10043. doi:10.1038/ncomms10043
33. D'Antona G, Ragni M, Cardile A, et al. Branched-chain amino acid supplementation promotes survival and supports cardiac and skeletal muscle mitochondrial biogenesis in middle-aged mice. *Cell Metab*. 2010;12:362–372. doi:10.1016/j.cmet.2010.08.016